water

MDPI

Article

Intelligent Methods for Estimating the Flood Susceptibility in the Danube Delta, Romania

Romulus Costache [1], Anca Crăciun [1,*], Nicu Ciobotaru [1] and Alina Bărbulescu [2,*]

[1] Danube Delta National Institute for Research and Development, 165 Babadag Street, 820112 Tulcea, Romania; romuluscostache2000@yahoo.com (R.C.); ciobotarunicu@gmail.com (N.C.)
[2] Department of Civil Engineering, Transilvania University of Brasov, 5, Turnului Street, 500152 Brasov, Romania
* Correspondence: anca.craciun@ddni.ro (A.C.); alina.barbulescu@unitbv.ro (A.B.)

Abstract: Floods, along with other natural and anthropogenic disasters, profoundly disrupt both society and the environment. Populations residing in deltaic regions worldwide are particularly vulnerable to these threats. A prime example is the Danube Delta (DD), located in the Romanian sector of the Black Sea. This research paper aims to identify areas within the DD that are highly or very highly susceptible to flooding. To accomplish this, we employed a combination of multicriteria decision-making (AHP) and artificial intelligence (AI) techniques, including deep learning neural networks (DLNNs), support vector machines (SVMs), and multilayer perceptron (MLP). The input data comprised previously flooded regions alongside eight geographical factors. All models identified high or very high flood potential of over 65% of the studied area. The models' performance was assessed using receiver operating characteristic (ROC) analysis, demonstrating excellent outcomes evaluated by the area under the curve (AUC) exceeding 0.908. This study is significant as it lays the groundwork for implementing measures against flood impacts in the DD.

Keywords: AHP; flood potential index; machine learning; MLP; SVM

Citation: Costache, R.; Crăciun, A.; Ciobotaru, N.; Bărbulescu, A. Intelligent Methods for Estimating the Flood Susceptibility in the Danube Delta, Romania. *Water* **2024**, *16*, 3511. https://doi.org/10.3390/w16233511

Academic Editor: Guoqing Wang

Received: 1 November 2024
Revised: 26 November 2024
Accepted: 4 December 2024
Published: 6 December 2024

1. Introduction

Floods lead to significant socioeconomic losses and environmental damage worldwide. Reducing flood risk and managing water resources in the face of global environmental changes presents a major challenge for contemporary society [1]. Floods are complex phenomena that can create varying levels of damage depending on the geographical conditions of the affected areas. Given the increasing frequency and severity of floods, accurately identifying flood risk areas is essential [2].

Every year, numerous regions face natural disasters linked to water in excess. Floods, in particular, rank as the most destructive among natural hazards, impacting nearly 200 million people worldwide annually [3,4]. During recent decades, there has been an important recorded increase in the frequency of these disasters [5,6], mostly attributed to the global climate change. This trend is expected to continue, resulting in more damages from floods [7]. In Europe, Romania ranks third after Italy and France in terms of the financial impact and casualties caused by these phenomena [8].

According to the European Directive on Floods 2007/60/EC [9], all actions aimed at reducing the adverse impacts of floods need to be grounded in the prior identification of areas most vulnerable to these natural hazards [10]. Assessing flood susceptibility in a region is also a critical non-structural measure for effective flood risk management. National hydrological forecasting centers issue flood forecasts and warnings by evaluating predicted precipitation and the area's susceptibility to flooding. To maximize the effectiveness of flood mitigation efforts, accurate assessment of flood potential in a given region is crucial.

In general, worldwide, floodplains and deltas are very sensitive to increased flows and river levels that can easily generate floods [11,12]. Flood susceptibility indices and

hydrodynamic modeling are very prevalent in the studies aimed to estimate areas affected by river flooding. It should be noted that river deltas are extremely vulnerable to environmental changes and natural disasters [13]. Therefore, it is crucial to examine the natural hazards that may impact the ecological systems of coastal environment and deltaic areas, with a particular focus on identifying areas susceptible to these phenomena.

In recent years, numerous models for estimating susceptibility to flooding have been proposed by the specialized scientific literature and have also been applied, including for deltaic areas [14–16]. Traditional hydrological techniques, like data-driven analysis and also rainfall-runoff models, cannot comprehensively analyze rivers and floodplains. Significant advancements in flood modeling and prediction have been achieved through the use of geographic information systems (GIS) and remote sensing [17]. Along with the increase in the number of papers dealing with this theme, there has also been a significant diversification of models applied to evaluate the flood hazard. From a qualitative point of view, in the specialized literature, flood hazard is expressed through the susceptibility or potential for the occurrence of these phenomena [10,18]. The first category of widely used methods for determining areas susceptible to flooding is multicriteria decisional analysis. This category includes the AHP, analytical network process, TOPSIS, and VIKOR methods [19,20]. Fuzzy systems have also been applied to identify the zones most prone to floods [21].

Both decisional multicriteria analysis and fuzzy systems are methods that rely on expert opinions, which introduce a certain degree of subjectivity [22]. In contrast, there are algorithms that do not rely on expert intervention; instead, their application is based solely on the available data [23]. Bivariate statistics, such as frequency ratios, evidence weights, the entropy index, and statistical indices, fall into this category. Additionally, various techniques from the field of artificial intelligence have been adapted for calculating flood susceptibility, including ANN and the ANFIS [24,25]. Another group of methods that relies exclusively on available data belongs to ML (a subfield of AI), which includes SVM, random forests (RFs), classification and regression trees, rotation forests, and naïve Bayes [26]. All of these models utilize datasets that contain the locations of past flood events along with a variable number of predictors [27]. The ability to evaluate a model's precision and verify the results is a significant benefit of using these methods to evaluate susceptibility to floods.

In Romania, most studies investigated water quality [28–30], a few articles utilized AI or hybrid methods for flood evaluation of some rivers [31–35], and only a limited number of studies [36,37] were dedicated to hydrological modeling for small zones in the DD biosphere reserve, which is the subject of this study. Therefore, the main goal of our article is determining the flood hazard in the DD biosphere reserve through AI methods. The study will highlight aspects that were not investigated until now, which will also contribute to a better understanding of the flooding mechanism and serve as a background for policymakers for insight into the measures that can be taken for flood prevention and the mitigation of their effects.

2. Data Series and Methodology

2.1. The Study Zone

The analyzed region is the DD (Figure 1), which was formed in the last 5200 years between the Bugeacului Plain and the Dobrogea Plateau. A morphological analysis classifies the DD as a developing alluvial plain, with reduced hypsometry. The maximum elevation range of 64 m is related to the region of the Letea fluvial sea dike and Tulcea Branch. The DD is formed by the deposition of sediments carried by the Danube River, creating a complex network of channels, lakes, islands, marshes, and reed beds. It constantly shifts, with new islands and channels forming, while older ones may disappear or become more saline over time.

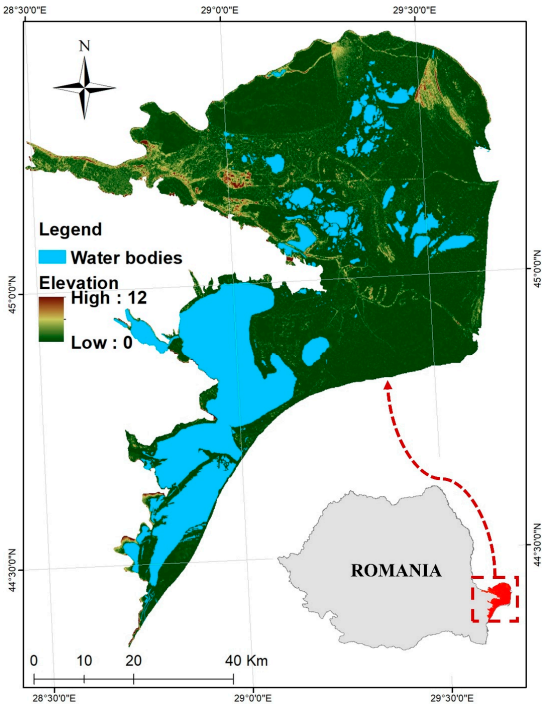

Figure 1. Map of the research zone.

The DD faces significant flood hazards due to its low-lying geography, the seasonal variability of the Danube River, and climate change. The delta's ecosystem stability is threatened by sea-level depth rise, temperature rising, and shifts in rainfall patterns. Its biodiversity is also at significant risk from increasingly frequent extreme meteorological phenomena like drought and floods.

2.2. Data Series

2.2.1. Inventory of Flooded Areas

In our pursuit of applying AI methods to understand the influence of geographical factors on flood occurrence, we identified the zones previously subjected to floods. We divided this dataset into training areas (70% of the total) and validation areas (30%). To ensure the highest degree of objectivity of the results, we randomly selected other dry areas within the DD, with a total area equal to those affected by floods. These were also split into training and validation zones (70–30%). Given that the flood susceptibility detection is a binary process, the first dataset used in the AI models, signifying the presence of flood phenomena, was coded with 1, while the second dataset, signifying the absence of flood phenomena, was coded with 0. The presence/absence of flood-affected areas will constitute the dependent variable within the AI models for flood-susceptible zones.

2.2.2. Flood Conditioning Factors

Identifying areas susceptible to flooding requires consideration of eight key factors that significantly influence flood occurrence: relief slope, altitude, distance from watercourses, land use, vertical distance from rivers, distance from water bodies, lithology, and soil hydrological group. The relief slope, elevation, and vertical distance from rivers are morphometric factors derived from the digital terrain model (DTM).

The study area's DTM was extracted utilizing the SRTM database. The other five factors were obtained by extracting or processing existing vector databases. Specifically, the distances to rivers and water bodies were calculated using the recorded hydrographic network of rivers and lakes. Additionally, the land use dataset was obtained from the Corine Land Cover 2018, while lithological information was sourced from the Geological Map of Romania in digital format at 1:200,000 scale. The spatial distribution of the soil

hydrological group in the DD was also represented using the Digital Soil Map of Romania at 1:200,000 scale. Below is a brief description of all eight geographic factors that were used in this research.

The slope of the relief can influence the flooding susceptibility in a given area. Slope angle refers to the steepness or gradient of the land surface and decisively influences surface runoff during a flood event [38]. Here, the slope categories are as follows: 0–1°, 1.1–2°, 2.1–3°, 3.1–4°, and >4° (Figure 2a).

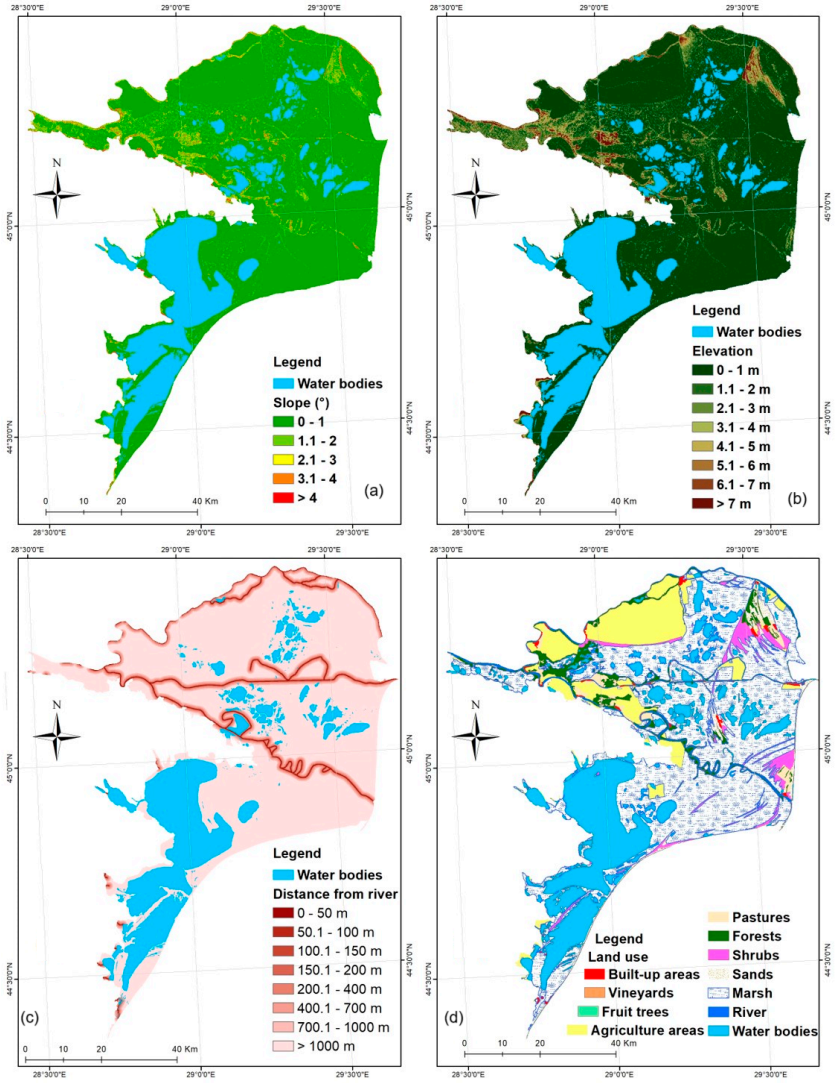

Figure 2. Factors conditioning the flooding (**a**) slope, (**b**) altitude, (**c**) distance to rivers, and (**d**) land use.

Elevation significantly impacts flood susceptibility. Zones having low altitudes are more exposed to flood genesis because of proximity to water bodies or their tendency to collect water during heavy rains [39]. In this study, eight classes were established for elevation: 0–1 m, 1–2 m, 2–3 m, 3–4 m, 4–5 m, 5–6 m, 6–7 m, and >7 m (Figure 2b).

Distance to rivers greatly influences flood susceptibility, with regions near rivers or within low-lying floodplains facing a higher risk [40]. Even distant low-lying zones can collect water during heavy rains, making them prone to flooding. Specific distance classes have been established to assess this factor: [0, 50), [50, 100), [100, 150), [150, 200), [200, 400), [400,700), [700, 1000), and above 100 m (Figure 2c).

Land use in deltaic regions can significantly impact flood susceptibility. The presence of impervious surfaces (roads and buildings) can increase the amount of runoff on the ground surface and contribute to flooding genesis [41]. According to the Corine Land

Cover database, 10 classes could be found in the DD (Figure 2d). Areas of the DD occupied by swamps that are not ecologically designed as floodwater retention areas can be highly flood-prone.

The vertical distance to the river affects flood susceptibility, and higher elevations above the drainage channel are less prone to flooding. However, areas in narrow valleys or steep slopes may still face risks due to rapid water drainage. In the DD, the altitude above the channel was categorized into the following specific groups: [0, 1), [1, 2), [2, 3), [3, 4), [4, 5), [5, 6), [6, 7), and greater than 7 m (Figure 3a).

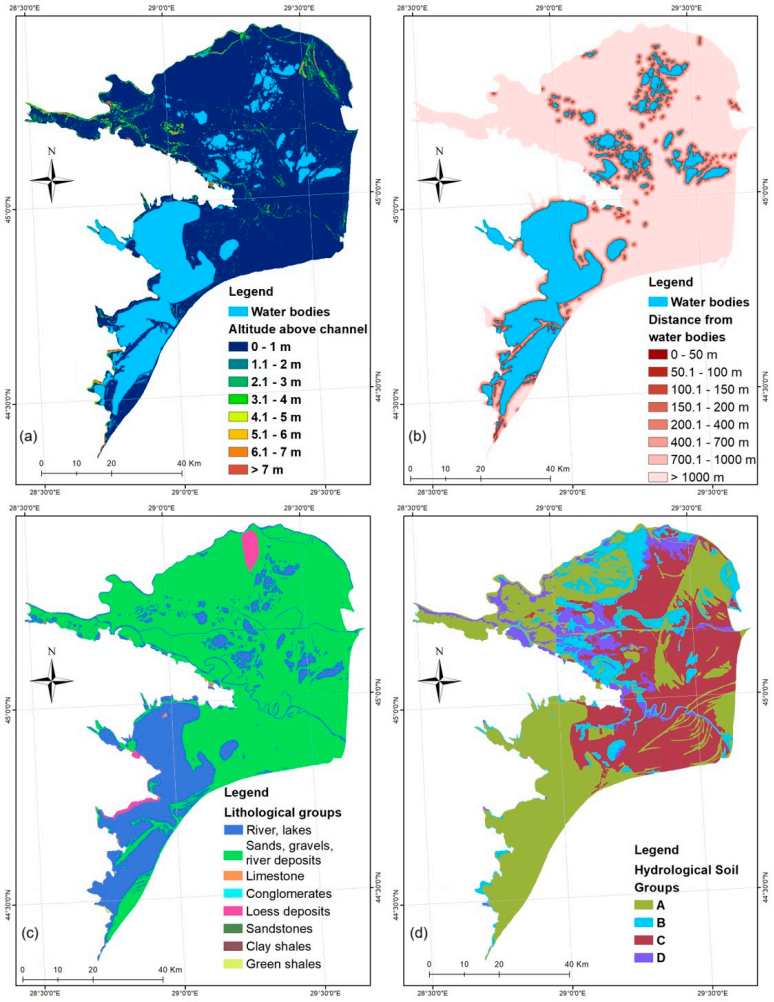

Figure 3. Factors conditioning the flood (**a**) vertical distance to rivers, (**b**) distance to water bodies, (**c**) lithology, and (**d**) hydrological soil group.

In the DD, water bodies cover vast areas, and any rise in their water levels poses a significant threat to surrounding regions. The distance to these water bodies was calculated using the Euclidean distance method. Eight distance classes (in meters) were established to define the proximity to water bodies: [0, 50), [50, 100), [100, 150), [150, 200), [200, 400), [400, 700), [700, 1000), and greater than 1000 m (Figure 3b).

Lithology influences flood susceptibility as different rock types vary in permeability. Impermeable rocks, like clay, increase surface runoff, raising flood risk, while permeable rocks, like sand or gravel, promote water infiltration, reducing risk [24]. Six lithological categories were identified in the DD (Figure 3c).

Soil type also impacts the rate of water infiltration, sometimes favoring the accumulation of water at the surface of the soil. For this study, the digital Romanian soil map at

a 1:200,000 scale was used as a data source. As shown in Figure 3d, all four hydrological groups are represented in the DD.

The classification of the following factors was based on expert judgment, which considered the study area's characteristics: slope, altitude, distance from water bodies, distance from rivers, and vertical distance to the river network. Land use, lithological groups, and hydrological soil groups were classified according to their categories.

2.3. Methodology

2.3.1. Information Gain (IG)

IG measures the reduction in uncertainty (entropy) of a target variable Y when a feature X is known. Here, Y is the location of flooded areas, while each conditioning factor represents X. Features with higher IG are considered more informative and are often selected for building predictive models.

IG was used to test each factor's predictive ability regarding rapid water runoff on slopes. This method reduces uncertainties by eliminating factors with a low predictive capacity.

The quality of a discrete attribute is defined as the expected decrease in impurity when the attribute value is known. Information gain is determined as the difference between the entropy of a class and the entropy of the same class conditioned by the attribute [42]. It should be noted that the IG results do not have general applicability, being influenced by the characteristics of the zone and the location of the dependent variable.

The IG values were determined in WEKA 3.9.2 software.

2.3.2. Analytical Hierarchy Process (AHP)

Given the importance of establishing weights as objectively as possible for the classes of factors that influence the potential for flood formation, the AHP method was used in the present study. This algorithm [43] allows for solving and analyzing a problem flexibly and easily. A key feature of this approach is the active involvement of specialists throughout the entire methodological process. AHP is commonly used in research aiming to assess susceptibility to natural risk phenomena [44]. The core of the methodology lies in breaking down complex problems into a hierarchical structure, placing at the top the main goal, with criteria and sub-criteria following at lower levels. At the bottom, the alternative decisions are situated.

Five main stages can be distinguished when using AHP to determine the coefficients of the factor classes within the study area:

(i) Divide the problem into several parts, then set the objectives.
(ii) Determine the criteria and alternatives.
(iii) Create a comparison matrix, X, for the pairs of factors that influence flood production, and the pairs composed of their respective categories or classes. X is built taking into account the expert judgment regarding the impact of each factor category/class on flooding potential. If one class/category is more significant than another, its relative value will range from 1 to 9 and be assigned horizontally. Conversely, when a class/category is less important, the values assigned horizontally will vary between 1/9 and 1/2.
(iv) Compute the relative weights of the factors category/class using the eigenvalue technique.
(v) Calculate the consistency ratio (CR) matrix, which shows the pairwise comparisons' quality. CR is obtained using Equation (2), which involves first calculating the consistency index (CI) from Equation (1):

$$CI = \frac{\lambda_{max} - n}{n - 1} \quad (1)$$

where λ_{max} is the highest eigenvalue and n is the number of factors conditioning the potential for flash floods, respectively.

$$CR = CI/RI \quad (2)$$

The number of categories/classes of the factors, and *RI* depend on the number of factors included in the comparison matrix (Table 1).

Table 1. *RI* [43].

n	3	4	5	6	7	8	9	10	11	12	13	14	15
RI	0.58	0.90	1.12	1.24	1.32	1.41	1.45	1.49	1.51	1.53	1.56	1.57	1.59

A qualitatively performing comparison matrix is indicated by a $CR < 0.1$.

All mathematical operations were performed in Microsoft Excel 2016 software, while maps and primary data related to geographic factors were obtained in ArcGIS 10.5.

The values of the AHP coefficients formed the input data in the AI algorithm to calculate the flood susceptibility within the DD.

2.3.3. DLNN

Deep learning (DL) belongs to of machine learning (ML) category, which utilizes AI networks to learn from large datasets. It relies on layers of neural networks, which are heavily inspired by brain functions. Training these networks with extensive data adjusts the configuration of neurons within the system. Once trained, a DL model can process new data. These models analyze information from various data sources in real-time, without human intervention.

Compared to basic ANNs, DLNNs feature a structure with multiple hidden layers composed of neurons. Whereas a simple neural network may have one or two hidden layers, a DLNN may have a high number of layers. Increasing this number and the nodes can improve the performance, but an increased number of parameters and computational resources are also required. DL processes and classifies information, each layer receiving the raw data as input [45,46].

In this study, the DLNN model was applied to estimate flood susceptibility. The flood conditioning factors served as input data in the input layer, while the dataset indicating the presence or absence of flooded areas was used as output data in the output layer. A sigmoid function, $E(Y = 1/x)$, was employed to classify pixels as either flooded or non-flooded. The output layer consisted of a single neuron for each class i, providing an approximation of $E(Y = i/x)$. The sum of all estimated values equaled 1. For this study, the *softmax* function was used for the final classification:

$$softmax(a_i) = \frac{\exp(a_i)}{\sum_k \exp(a_i)} \quad (3)$$

where a_i is a layer of the *softmax* function.

A neural network with multiple hidden layers (h) can be expressed utilizing the following mathematical relations:

$$a^{(h)}(x) = b^{(h)} + W^{(h)} p^{(h-1)}(x), \quad (4)$$

$$p^{(h)}(x) = \varnothing(a^{(h)}(x)) \quad (5)$$

where $\varnothing$ is the activation function, and for $h = 1, \ldots, H$ (hidden layers).

The TensorFlow2.0 platform and Keras in Python 3.13.1 were used to run the DLNN model.

2.3.4. Support Vector Machine

SVM is a robust, supervised mathematical ML algorithm widely used in training dataset classification. It is primarily a binary classification technique that identifies an

optimal hyperplane in an n-dimensional space based on the training data. This hyperplane is then used to classify new datasets, effectively dividing the training data into two distinct classes.

To classify multidimensional data, SVM employs "kernels" that enable the construction of multidimensional hyperplanes. A hyperplane acts as a boundary that separates data points, serving as a decision boundary between the two classes. When there are two input variables, the hyperplane is represented as a straight line; if there are more than two inputs, it becomes a plane in higher dimensions.

Support vectors are the data points that play a crucial role in optimizing the hyperplane. These vectors are positioned closest to the hyperplane and represent the most challenging cases to classify. The location of the decision hyperplane is directly influenced by the SVs. If these SVs are removed, the position of the hyperplane will change as a result [47]. The inputs and outputs of an SVM are similar to those of a neural network. Constructing an optimized hyperplane in a linearly separable problem is done using Kernels functions.

2.3.5. Multilayer Perceptron (MLP)

An MLP [48] is an ANN formed by multiple layers of neurons, among which is an input and output layer and one or many hidden layers. Hidden layers are formed of interconnected neurons and have the role of processing the input data. All neurons from a hidden layer receive information from all neurons from the previous layer. Each input value is multiplied by a certain weight, influencing the output. A bias is also associated with each neuron. During the training phase, the biases and weights are learned, and the output of each neuron in a hidden or output layer is obtained by computing the weighted sum of the inputs plus the bias. Training the network is done by a backpropagation algorithm aiming to minimize the root mean square error (RMSE). RMSE values close to 0 highlight the models' good performance.

2.3.6. ROC Curve for Results Validation

The ROC curve is built in orthogonal coordinates, where the *X*-axis contains the specificity and the *Y*-axis the sensitivity. It is used to measure the efficiency of a model. The larger the AUC, the better the model. The following reference intervals are considered for AUC: [0.9, 1]—the model is excellent, [0.8, 0.9)—very good, [0.7, 0.8)—good, [0.6, 0.7)—fair; values under 0.6 lead to the model's rejection [49].

The workflow for the present research is shown in Figure 4.

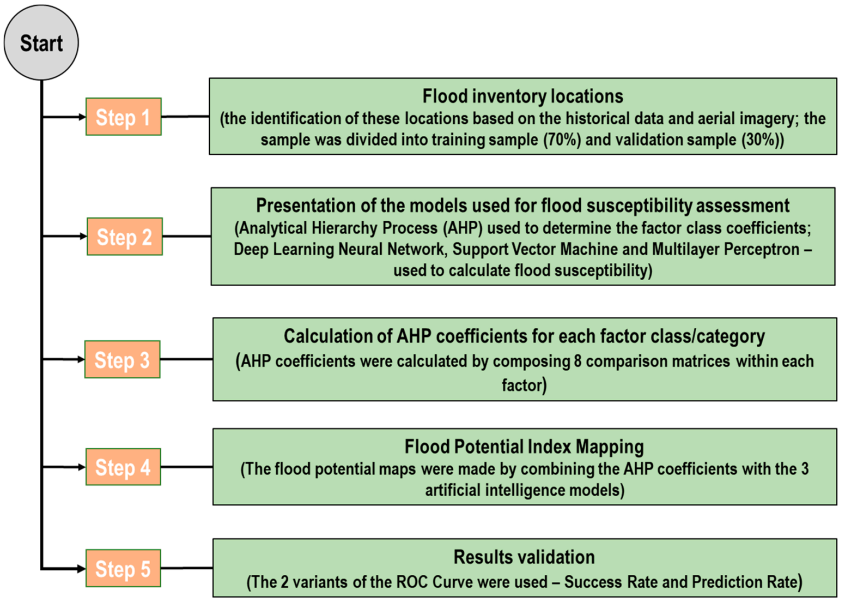

Figure 4. Workflow diagram.

3. Results

3.1. Information Gain Results

After applying the IG, it was found that the slope of the relief had the highest predictability for flood events, with an indicator value of 0.67. The vertical distance from nearby rivers was identified as the second most significant factor, with a value of 0.53. The hierarchy of the remaining factors is as follows: Altitude (0.41), Land use (0.36), Distance from rivers (0.29), Lithology (0.27), Distance from water bodies (0.22), and Hydrological soil groups (0.15) (Figure 5). Overall, the results from this method indicate that all eight geographic factors analyzed have some capacity to influence flooding events. Therefore, all eight variables will be considered for further analysis.

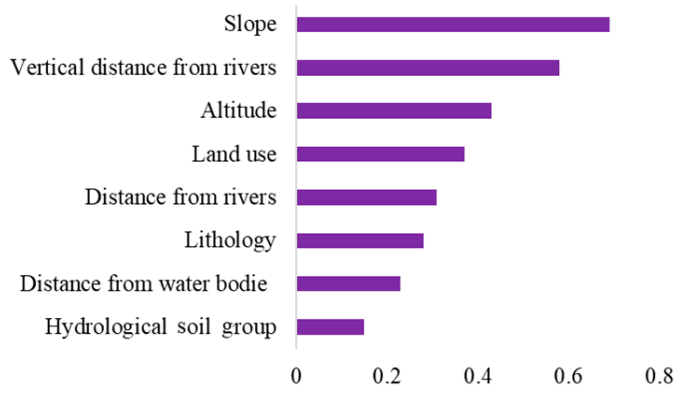

Figure 5. IG values.

3.2. Analytical Hierarchy Process Results

Table 2 contains all the possible combinations made between the classes/categories of geographical factors that condition the occurrence of floods. Each factor or class/category was compared to the others by assigning a dominant relative value, based on insights from the specialized literature [50]. The corresponding weights are provided in Table 2.

Table 2. AHP matrices used for factor weighting and factor classes/categories.

Factors/Classes Categories	**Pair-Wise Comparison**								**AHP**
Class/Categories	**[1]**	**[2]**	**[3]**	**[4]**	**[5]**	**[6]**	**[7]**	**[8]**	**Weights**
Slope (°)									
[1] 0–1	1	4	6	7	9				0.546
[2] 1–2	1/4	1	3	4	6				0.229
[3] 2–3	1/6	1/3	1	2	4				0.113
[4] 3–4	1/7	1/4	1/2	1	3				0.075
[5] >4	1/9	1/6	1/4	1/3	1				0.037
Altitude (m)									
[1] 0–1	1	2	3	4	5	6	7	8	0.327
[2] 1–2	1/2	1	2	3	4	5	6	7	0.227
[3] 2–3	1/3	1/2	1	2	3	4	5	6	0.157
[4] 3–4	1/4	1/3	1/2	1	2	3	4	5	0.108
[5] 4–5	1/5	1/4	1/3	1/2	1	2	3	4	0.073
[6] 4–6	1/6	1/5	1/4	1/3	1/2	1	2	3	0.050
[7] 6–7	1/7	1/6	1/5	1/4	1/3	1/2	1	2	0.034
[8] >7	1/8	1/7	1/6	1/5	1/4	1/3	1/2	1	0.024

Table 2. *Cont.*

Factors/Classes Categories	**Pair-Wise Comparison**								**AHP**
Class/Categories	**[1]**	**[2]**	**[3]**	**[4]**	**[5]**	**[6]**	**[7]**	**[8]**	**Weights**
Distance from river (m)									
[1] 0–50	1	2	3	4	5	6	7	9	0.323
[2] 50–100	1/2	1	2	3	4	5	6	7	0.221
[3] 100–150	1/3	1/2	1	2	3	4	5	6	0.152
[4] 150–200	1/4	1/3	1/2	1	2	3	4	5	0.104
[5] 200–400	1/5	1/4	1/3	1/2	1	3	3	3	0.073
[6] 400–700	1/6	1/5	1/4	1/3	1/3	1	4	6	0.063
[7] 700–1000	1/7	1/6	1/5	1/4	1/3	1/4	1	6	0.043
[8] >1000	1/9	1/7	1/6	1/5	1/3	1/6	1/6	1	0.021
Land use									
[1] Forests, sands	1	1/3	1/5	1/7	1/9				0.035
[2] Vineyards, fruit trees, shrubs	3	1	1/3	1/5	1/7				0.069
[3] Agriculture areas	5	3	1	1/3	1/5				0.136
[4] Pastures	7	5	3	1	1/2				0.286
[5] Built-up areas, marsh, river, water bodies	9	7	5	2	1				0.474
Altitude above channel (m)									
[1] 0–1	1	2	3	4	5	6	7	8	0.327
[2] 1–2	1/2	1	2	3	4	5	6	7	0.227
[3] 2–3	1/3	1/2	1	2	3	4	5	6	0.157
[4] 3–4	1/4	1/3	1/2	1	2	3	4	5	0.108
[5] 4–5	1/5	1/4	1/3	1/2	1	2	3	4	0.073
[6] 4–6	1/6	1/5	1/4	1/3	1/2	1	2	3	0.050
[7] 6–7	1/7	1/6	1/5	1/4	1/3	1/2	1	2	0.034
[8] >7	1/8	1/7	1/6	1/5	1/4	1/3	1/2	1	0.024
Distance from water bodies (m)									
[1] 0–50	1	2	3	4	5	6	8	9	0.324
[2] 50–100	1/2	1	2	3	4	5	7	8	0.225
[3] 100–150	1/3	1/2	1	2	3	4	6	7	0.156
[4] 150–200	1/4	1/3	1/2	1	2	4	5	6	0.113
[5] 200–400	1/5	1/4	1/3	1/2	1	2	3	4	0.069
[6] 400–700	1/6	1/5	1/4	1/4	1/2	1	2	6	0.053
[7] 700–1000	1/8	1/7	1/6	1/5	1/3	1/2	1	6	0.040
[8] >1000	1/9	1/8	1/7	1/6	1/4	1/6	1/6	1	0.019
Lithology									
[1] Sands, gravels, river deposits	1	1/2	1/4	1/6	1/9				0.043
[2] Loess deposits	2	1	1/2	1/3	1/4				0.090
[3] Limestone, conglomerates	4	2	1	1/2	1/5				0.142
[4] Clay shale, green shale	6	3	2	1	1/2				0.256
[5] Sandstone	9	4	5	2	1				0.469
Hydrological soil groups									
[1] A	1	3/4	1/2	1/5					0.108
[2] B	4/3	1	3/4	1/3					0.157
[3] C	2	4/3	1	1/3					0.201
[4] D	5	3	3	1					0.534

It can be seen that the highest AHP coefficient is assigned to slopes between 0° and 1°, which is equal to 0.546. A high value of this type of coefficient, of 0.534, was also obtained by soil hydrological group D. This factor class was followed by swamps within the land use mode, with a value of 0.474, and by the lithological category represented by sandstones, with a value of 0.469. Also, areas located far from watercourses below 50 m (0.362) and altitudes below 1 m (0.327) are considered categories of factors with high values of AHP coefficients.

CR values were involved in the quality assessment of matrices comparison procedure (Table 3). The *CR* values for all eight comparison matrices are below 0.1, indicating a high-quality analysis. Additionally, the table includes the values for the other parameters discussed in the theoretical section of the AHP model. These AHP coefficient values were

then used as input data in the AI models to identify the final flood-prone areas within the DD.

Table 3. Properties of AHP pair-wise comparison matrices.

Factors	No. of Factors/Classes	λ_{max}	*CI*	*RI*	*CR*
All factors	8	8.067	0.010	1.41	0.007
Slope	5	5.223	0.056	1.12	0.050
Elevation	8	8.048	0.007	1.41	0.005
Distance from river	8	8.351	0.050	1.41	0.036
Land use	5	5.223	0.056	1.12	0.050
Altitude above channel	8	8.048	0.007	1.41	0.005
Distance from water bodies	8	8.351	0.050	1.41	0.036
Lithology	5	5.223	0.056	1.12	0.050
Hydrological soil groups	4	4.011	0.004	0.90	0.004

3.3. DLNN Results

To train the DLNN model, a maximum of 100 epochs were set. For the training set, the minimum value of the loss parameter, equal to 0.0746, was reached after 99 epochs. The same situation was recorded for the validation set. In this regard, there were several parameters used: ReLU activation function, uniform kernel initialization function, a dropout rate of 0.1, a lot dimension of 100, a validation rate of 0.3, eight input neurons, a maximum of 100 hidden neurons, three hidden layers, and two output neurons. The architecture of DLNN, containing the input, hidden, and output layers, is represented in Figure 6.

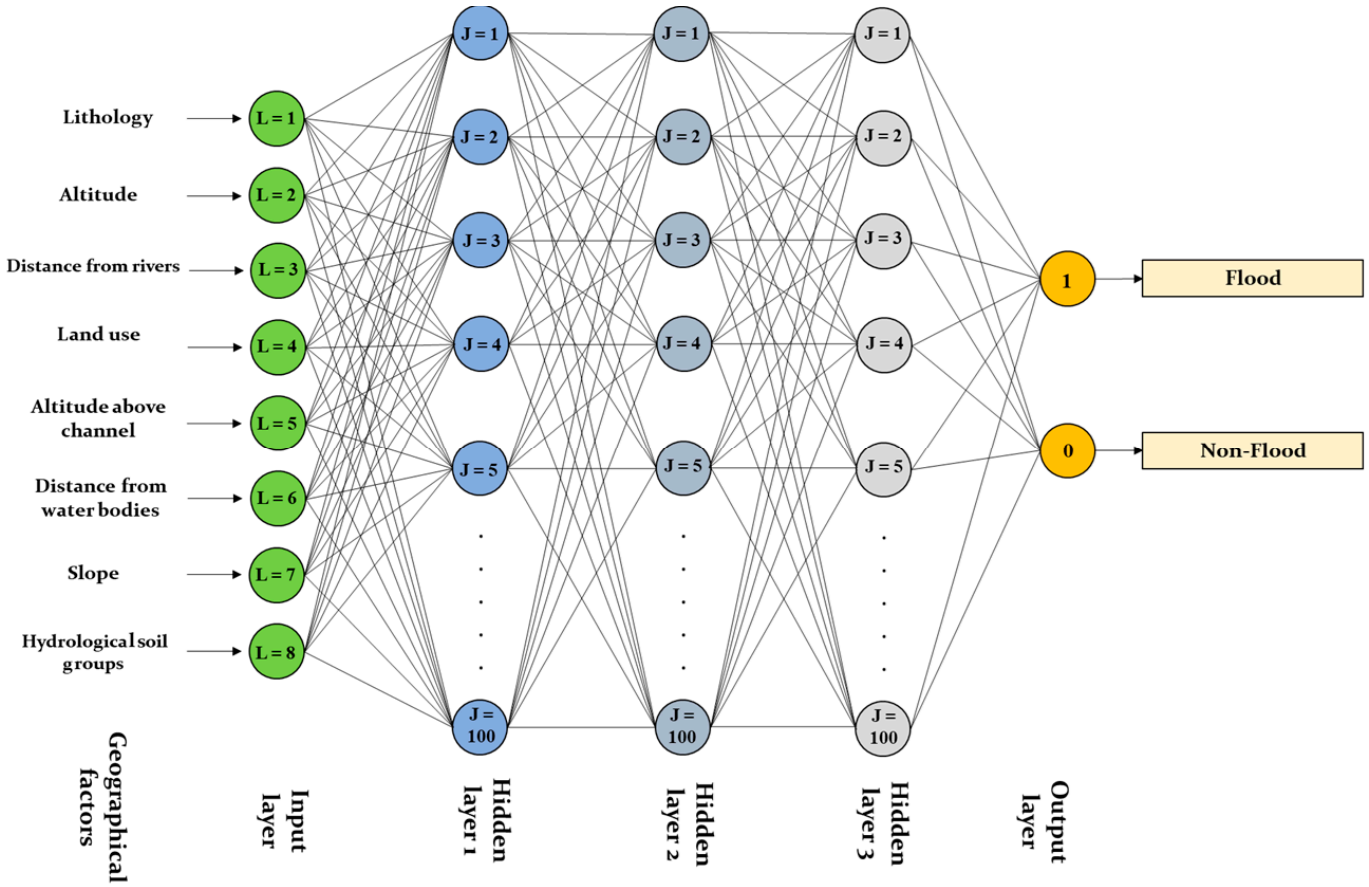

Figure 6. Architecture of the DLNN model used to determine flood susceptibility.

After training the model, the weights of each geographic factor used in this step were determined. Thus, the relief slope got the highest weight (0.241), followed by elevation (0.212), distance to rivers (0.173), land use (0.148), vertical distance to rivers (0.102), distance

to water bodies (0.069), lithology (0.029), and soil hydrologic group (0.026) (Figure 7). Utilizing cartographic algebra, these weights were multiplied by the AHP coefficients, after which the products resulting from the multiplication were added. Thus, the spatialized values of the susceptibility to floods, represented by the FPI, resulted (Figure 8a).

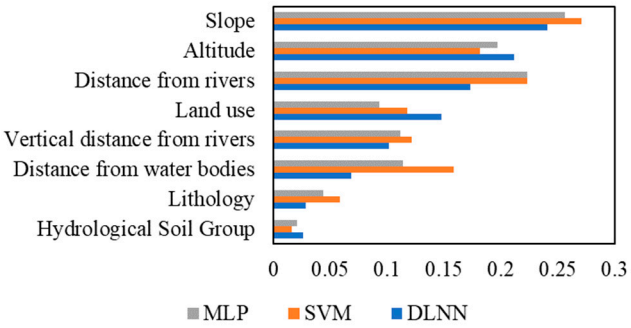

Figure 7. The weight of the geographic factors in the AI models.

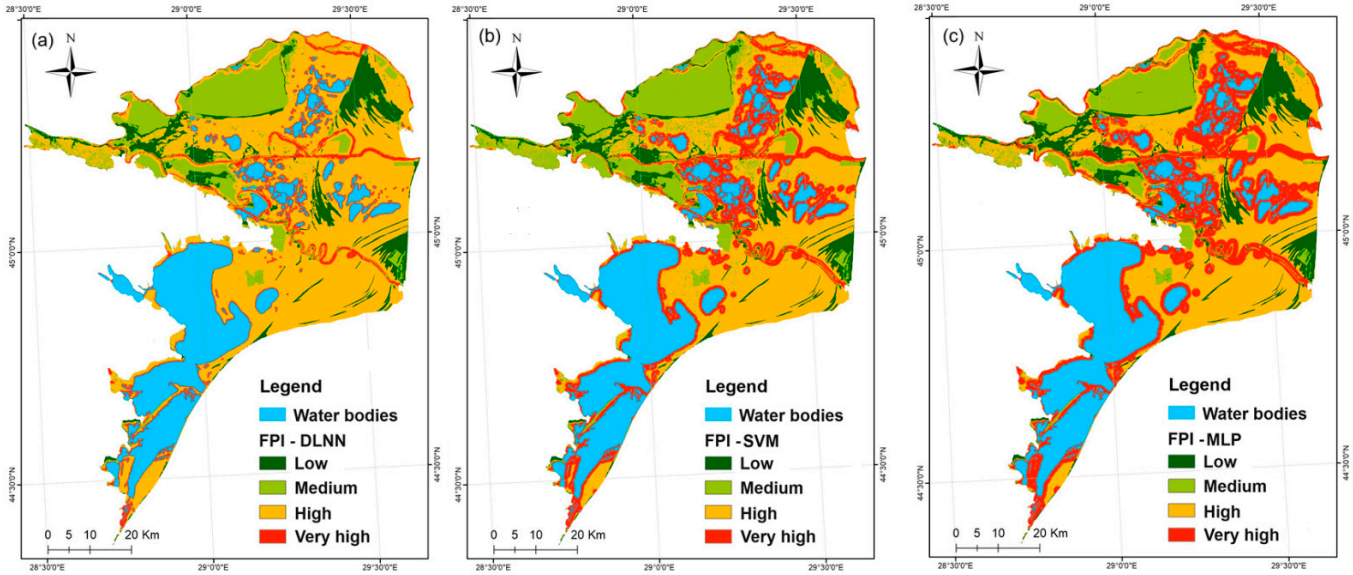

Figure 8. FPI (**a**) DLNN, (**b**) SVM, and (**c**) MLP.

The FPI-DLNN values were grouped into four classes using the natural breaks method. The first class refers to the reduced flood susceptibility values within the DD, which covers the higher areas, represented mainly by beams. The share of this class is 15% of the total study area (Figure 9). Next, the average flood susceptibility class is mainly distributed in the northern area of the DD. Overall, a percentage of 20% of the territory subject to research is moderately prone to flooding.

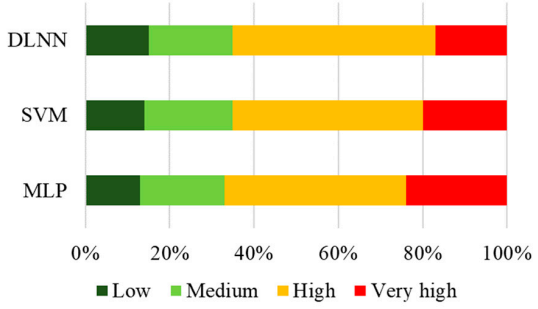

Figure 9. Weight of FPI classes calculated through ML methods.

The highest surface is occupied by areas with a high flood potential, which extend to about 48% of the study area. The areas characterized by a very high susceptibility to flooding are mainly located along the main watercourses in the study area. They extend over approximately 17% of the total territory occupied by the DD.

3.4. SVM Model Results

As with DLNN, the AHP values for each geographic factor class and category were used as input data within the SVM model. The accuracy of the results provided by SVM depends on the correct selection of the kernel function and the estimation of two parameters, C and γ, through the cross-validation procedure. The value of the parameter C was estimated at 2.1, and the value of γ was equal to 0.2. This pair of values shows a very well-optimized SVM model [51]. Once the training procedure was completed, the weights associated with the geographical factors could also be determined. Again, the slope of the relief obtained the highest importance (0.271), followed by the distance from rivers (0.223), altitude (0.182), distance from water bodies (0.159), vertical distance from rivers (0.122), land use (0.118), lithology (0.059), and soil hydrologic group (0.016). Like in the DLNN case, the spatialization of the FPI values was also achieved (Figure 8b) through cartographic algebra.

To compare the model's results, the values were again grouped into four classes using the natural breaks method. The lowest share, equal to 14%, can be attributed to areas where the susceptibility to flooding has a low value. Beams occupy the areas with higher altitudes than the surrounding regions. The average FPI extends mainly in the study area's northern half and occupies 21% of the total. A high susceptibility to flooding characterizes the equivalent of 45% of the DD, while the very high potential areas, represented on the map in red, have a weight of 20%.

3.5. MLP Model Results

To apply MLP, an architecture with eight neurons in the input layer, a maximum of 100 hidden neurons, and two neurons in the output layer (representing the presence or absence of flooding) was used (Figure 10). After the training process, RMSE reached its minimum value of 0.014 (Figure 11a) for 43 hidden neurons. The estimated pseudo-likelihood parameter indicates the accuracy of the classification process. A significant presence of values below 0.2 (for true positives) or above 0.8 (for false positives) in both flood and non-flood locations (areas where no floods occurred) indicates good classification accuracy. As shown in Figure 11b, these two classifications (floods and non-floods) are prominently present within the specified intervals, suggesting that the classification operation performed using the MLP model is highly accurate.

After training the MLP model, we derived the weights of the geographic factors used to assess flood susceptibility in the DD.

The factor with the highest weight was slope, at 0.256, followed by distance from rivers at 0.223, altitude at 0.197, distance from water bodies at 0.114, vertical distance from rivers at 0.112, land use at 0.093, lithology at 0.044, and soil hydrologic group at 0.021. Using the weights of these eight geographic factors in cartographic algebra, we calculated the flood potential index (FPI) through the MLP model. The final results were categorized into four value classes using the natural breaks method, as illustrated in Figure 8.

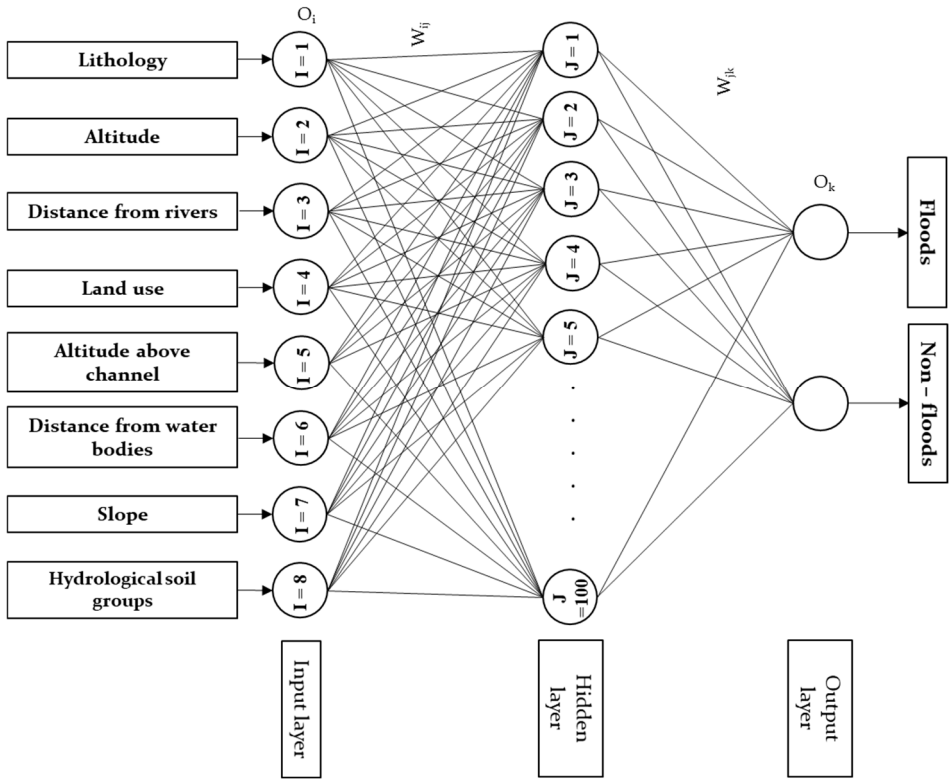

Figure 10. Architecture of the MLP model used to determine flood susceptibility.

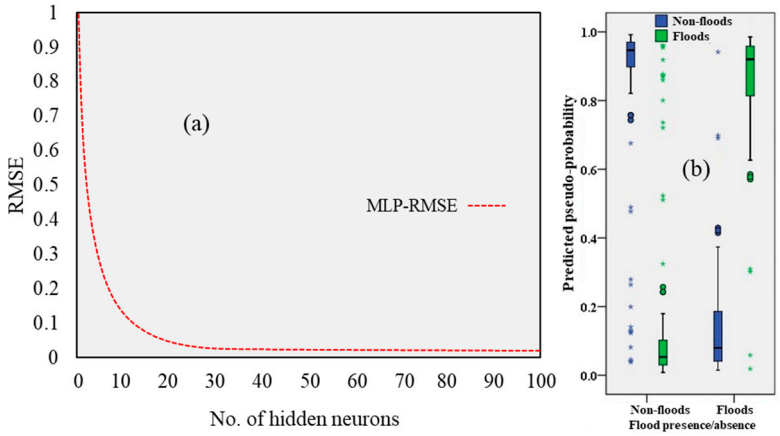

Figure 11. (**a**) Evolution of RMSE with respect to the number of hidden neurons and (**b**) estimated pseudo-likelihood for MLP.

3.6. Results Validation Using ROC Curve

The ROC curve was constructed for two variants: the success rate and the prediction rate, using SPSS 21 software. The success rate was calculated using the training sample and indicates how effectively the AI model classified the results. As shown in Figure 12a, the model with the highest performance was the DLNN, with an AUC of 0.963. The SVM followed it with an AUC of 0.954, and the MLP with an AUC of 0.939. All models performed well, as their AUC values were greater than 0.8.

The prediction rate was also determined using the test set. SVM provided the best results with an AUC of 0.942, followed by the DLNN with an AUC of 0.924 and the MLP with an AUC of 0.908 (Figure 12b). All models achieved an AUC value greater than 0.8 in the prediction rate analysis.

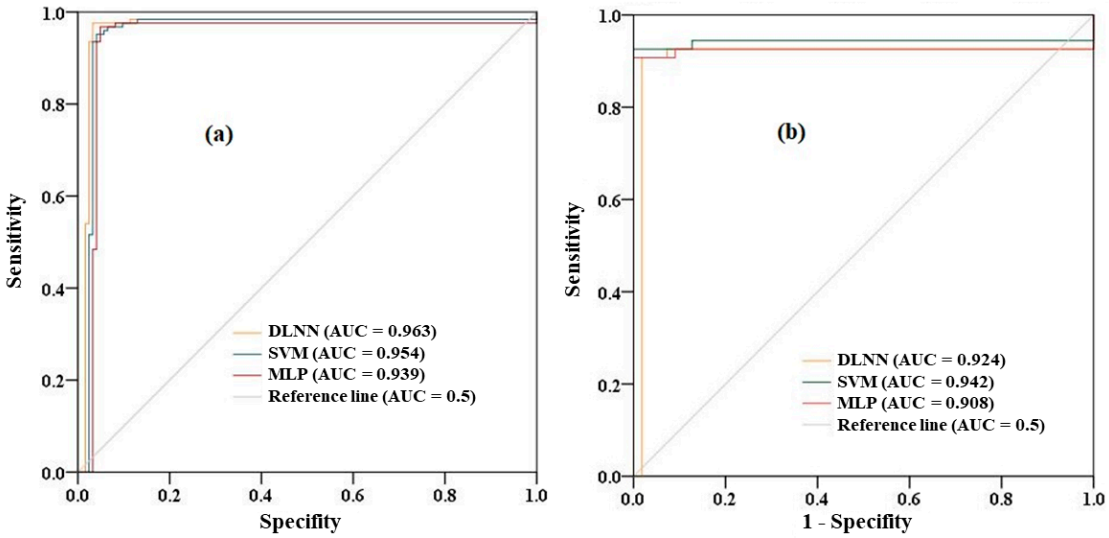

Figure 12. ROC curve (**a**) success rate and (**b**) prediction rate.

4. Discussion

The present workflow and the methodology proposed in this study represent a faster alternative to determine the flood hazard than hydraulic modeling. One of the study area's most famous flood risk assessment projects is the Danube FloodRisk Project, led by the Ministry of Environment from Romania and directly supervised by the International Commission for the Protection of the Danube River (ICPDR). Within this project, flood maps were generated through hydraulic modeling (a quantitative approach) for different river discharges determined based on statistical analysis (return periods: 30 years, 100 years, and 1000 years). Also, three classes of hazards were established according to the flood depth. Meanwhile, in the case of the current study, a qualitative approach was adopted to determine the susceptibility to floods, resulting from the overlap of several factors that influence the formation of this hydrological hazard. Unlike the project mentioned above, in this article, four classes were used to spatialize the severity of the hazard. Although the approaches differ, the results offered by them are, to a certain extent, similar. Thus, the highest flood hazard values are located along the main elements of the hydrographic network (the Danube arms and canals), and the lowest occur in the highest areas related to the banks. Flooding maps of the DD were also made within Cycle 1 of implementing the provisions of the Flood Directive 2007/60/EC of the European Commission. In this case, hydraulic modeling methods were also used to estimate the hazard's spatial variability. The results are very close to those of the Danube Flood Risk Project.

5. Conclusions

In this article, a DLNN, SVM, and MLP were used to qualitatively determine the hazard (susceptibility) to flooding within the Danube Delta based on information regarding the presence or absence of flood phenomena at the study area's level and data regarding the spatial values of eight geographic factors. All models revealed that the relief slope has the most significant influence on the flood phenomenon. Information gain was employed to test the predictive capacity of each geographic factor in flood genesis. Once this capacity was confirmed, the AHP coefficients that fed into the models were determined. A key aspect was validating the results using the ROC curve method, which confirmed that all models had an accuracy of over 90%.

Applying the entire workflow to determine the flood hazard qualitatively allowed the following output to be obtained:

- A GIS database with the training and validation samples comprising flood-affected areas in the DD reserve and an equal number of pixels with non-flood-affected areas.

- A GIS database with the eight geographical factors that influence the occurrence of floods within the study zone.
- An Excel tabular template with the AHP method that can also be applied to other study areas.
- A GIS database with the three susceptibility indices to flooding within the DD. According to the results provided by the three indices, approximately 65–70% of the DD's surface has a high or very high risk of flooding.

Moreover, the approach also represents the study's novelty in using techniques—ML algorithms combined with multicriteria decision-making analysis—that have not been used until now to evaluate the susceptibility to flooding in the DD. This research is also important because the DD represents one of the natural regions of Europe, having been declared a biosphere reserve and included in the UNESCO World Heritage List. The authorities can focus on finding the most environmentally friendly flood mitigation measures based on it.

The present research results are closely related to both facades of flood sustainability: sustainable management of floods and long-term flood resilience. The sustainable management of floods refers to strategies and practices harmonizing flood mitigation efforts with ecological conservation. Examples include maintaining the natural functioning of floodplains, implementing green infrastructure, and cultivating flood-resistant crops in agricultural areas. Meanwhile, long-term flood resilience emphasizes enabling societies and environments to recover from floods while sustaining essential functions, including planning for sustainable development in flood-prone regions and building resilient infrastructure.

Author Contributions: Conceptualization, R.C., A.C., N.C., and A.B.; methodology, R.C., A.C., N.C., and A.B.; software, R.C., A.C., and N.C.; validation, R.C.; formal analysis, R.C., N.C., and A.B.; investigation, R.C.; resources, R.C., A.C., and N.C.; data curation, R.C.; writing—original draft preparation, R.C., A.C., and N.C.; writing—review and editing, R.C., N.C., and A.B.; visualization, R.C., N.C., and A.B.; supervision, R.C.; project administration, R.C.; funding acquisition, R.C. and A.B. All authors have read and agreed to the published version of the manuscript.

Funding: This research was funded by the Ministry of Research, Innovation, and Digitization within the framework of Nucleus Program "DD 2030" PN 23 13, 2023–2026—Nucleus Project: "Research on the contribution of ecological restoration activities in the management of environmental risks caused by global climate change in the DD Biosphere Reserve—PN 23 13 02 01".

Data Availability Statement: The datasets generated during and/or analyzed during the current study are available from the corresponding author on reasonable request.

Conflicts of Interest: The authors declare no conflicts of interest.

References

1. Zhao, J.; Zhang, Q.; Xu, L.; Sun, S.; Wang, G.; Singh, V.P.; Wu, W. Flood-susceptible areas within the Yellow River Basin, China: Climate changes or socioeconomic behaviors. *J. Hydrol. Reg. Stud.* **2024**, *55*, 101900. [CrossRef]
2. Amiri, A.; Soltani, K.; Ebtehaj, I.; Bonakdari, H. A novel machine learning tool for current and future flood susceptibility mapping by integrating remote sensing and geographic information systems. *J. Hydrol.* **2024**, *632*, 130936. [CrossRef]
3. Acquaotta, F.; Faccini, F.; Fratianni, S.; Paliaga, G.; Sacchini, A.; Vilímek, V. Increased flash flooding in Genoa Metropolitan Area: A combination of climate changes and soil consumption? *Meteorol. Atmos. Phys.* **2019**, *131*, 1099–1110. [CrossRef]
4. Khosravi, K.; Shahabi, H.; Pham, B.T.; Adamowski, J.; Shirzadi, A.; Pradhan, B.; Dou, J.; Ly, H.-B.; Gróf, G.; Ho, H.L. A comparative assessment of flood susceptibility modeling using Multi-Criteria Decision-Making Analysis and Machine Learning Methods. *J. Hydrol.* **2019**, *573*, 311–323. [CrossRef]
5. Arnell, N.W.; Gosling, S.N. The impacts of climate change on river flood risk at the global scale. *Clim. Chang.* **2016**, *134*, 387–401. [CrossRef]
6. Swain, K.C.; Singha, C.; Nayak, L. Flood susceptibility mapping through the GIS-AHP technique using the cloud. *ISPRS Int. J. Geo Inf.* **2020**, *9*, 720. [CrossRef]
7. Bubeck, P.; Botzen, W.J.; Aerts, J.C. A review of risk perceptions and other factors that influence flood mitigation behavior. *Risk Anal.* **2012**, *32*, 1481–1495. [CrossRef]
8. Vinke-de Kruijf, J.; Kuks, S.M.; Augustijn, D.C. Governance in support of integrated flood risk management? The case of Romania. *Environ. Develop.* **2015**, *16*, 104–118. [CrossRef]

9. European Directive on Floods 2007/60/EC. Available online: https://www.legislation.gov.uk/eudr/2007/60 (accessed on 24 October 2024).
10. Arora, A.; Arabameri, A.; Pandey, M.; Siddiqui, M.A.; Shukla, U.; Bui, D.T.; Mishra, V.N.; Bhardwaj, A. Optimization of state-of-the-art fuzzy-metaheuristic ANFIS-based machine learning models for flood susceptibility prediction mapping in the Middle Ganga Plain, India. *Sci. Total Environ.* **2021**, *750*, 141565. [CrossRef]
11. Vogel, A.; Seeger, K.; Brill, D.; Brückner, H.; Kyaw, A.; Myint, Z.N.; Kraas, F. Towards Integrated Flood Management: Vulnerability and Flood Risk in the Ayeyarwady Delta of Myanmar. *Int. J. Disaster Risk Reduct.* **2024**, *114*, 104723. [CrossRef]
12. Guven, D.S.; Yenigun, K.; Isinkaralar, O.; Isinkaralar, K. Modeling flood hazard impacts using GIS-based HEC-RAS technique towards climate risk in Şanlıurfa, Türkiye. *Nat. Hazards* **2024**, 1–19. [CrossRef]
13. Zhu, K.; Lai, C.; Wang, Z.; Zeng, Z.; Mao, Z.; Chen, X. A novel framework for feature simplification and selection in flood susceptibility assessment based on machine learning. *J. Hydrol. Reg. Stud.* **2024**, *52*, 101739. [CrossRef]
14. Dottori, F.; Szewczyk, W.; Ciscar, J.-C.; Zhao, F.; Alfieri, L.; Hirabayashi, Y.; Bianchi, A.; Mongelli, I.; Frieler, K.; Betts, R.; et al. Increased human and economic losses from river flooding with anthropogenic warming. *Nat. Clim. Chang.* **2018**, *8*, 781–786. [CrossRef]
15. Pradhan, B. Remote sensing and GIS-based landslide hazard analysis and cross-validation using multivariate logistic regression model on three test areas in Malaysia. *Adv. Space Resear.* **2010**, *45*, 1244–1256. [CrossRef]
16. Anand, A.K.; Pradhan, S.P. Evaluation of bivariate statistical and hybrid models for the preparation of flood hazard susceptibility maps in the Brahmani River Basin, India. *Environ. Earth Sci.* **2023**, *82*, 389. [CrossRef]
17. Wang, W.; Sang, G.; Zhao, Q.; Liu, Y.; Shao, G.; Lu, L.; Xu, M. Prediction of flash flood peak discharge in hilly areas with ungauged basins based on machine learning. *Hydrol. Resear.* **2024**, *55*, 801–814. [CrossRef]
18. Abdulrazzak, M.; Elfeki, A.; Kamis, A.; Kassab, M.; Alamri, N.; Chaabani, A.; Noor, K. Flash flood risk assessment in urban arid environment: Case study of Taibah and Islamic universities' campuses, Medina, Kingdom of Saudi Arabia. *Geomat. Nat. Hazards Risk* **2019**, *10*, 780–796. [CrossRef]
19. Rafiei-Sardooi, E.; Azareh, A.; Choubin, B.; Mosavi, A.H.; Clague, J.J. Evaluating urban flood risk using hybrid method of TOPSIS and machine learning. *Int. J. Disaster Risk Reduct.* **2021**, *66*, 102614. [CrossRef]
20. Dutta, P.; Deka, S. A novel approach to flood risk assessment: Synergizing with geospatial based MCDM-AHP model, multi-collinearity, and sensitivity analysis in the Lower Brahmaputra Floodplain, Assam. *J. Clean. Prod.* **2024**, *467*, 142985. [CrossRef]
21. Ahmadlou, M.; Karimi, M.; Alizadeh, S.; Shirzadi, A.; Parvinnejhad, D.; Shahabi, H.; Panahi, M. Flood susceptibility assessment using integration of adaptive network-based fuzzy inference system (ANFIS) and biogeography-based optimization (BBO) and BAT algorithms (BA). *Geocarto Int.* **2019**, *34*, 1252–1272. [CrossRef]
22. Termeh, S.V.R.; Kornejady, A.; Pourghasemi, H.R.; Keesstra, S. Flood susceptibility mapping using novel ensembles of adaptive neuro fuzzy inference system and metaheuristic algorithms. *Sci. Total Environ.* **2018**, *615*, 438–451. [CrossRef] [PubMed]
23. Wang, Y.; Hong, H.; Chen, W.; Li, S.; Panahi, M.; Khosravi, K.; Shirzadi, A.; Shahabi, H.; Panahi, S.; Costache, R. Flood susceptibility mapping in Dingnan County (China) using adaptive neuro-fuzzy inference system with biogeography based optimization and imperialistic competitive algorithm. *J. Environ. Manag.* **2019**, *247*, 712–729. [CrossRef] [PubMed]
24. Bui, D.T.; Tsangaratos, P.; Ngo, P.-T.T.; Pham, T.D.; Pham, B.T. Flash flood susceptibility modeling using an optimized fuzzy rule based feature selection technique and tree based ensemble methods. *Sci. Total Environ.* **2019**, *668*, 1038–1054. [CrossRef]
25. Pham, B.T.; Shirzadi, A.; Bui, D.T.; Prakash, I.; Dholakia, M. A hybrid machine learning ensemble approach based on a radial basis function neural network and rotation forest for landslide susceptibility modeling: A case study in the Himalayan area, India. *Int. J. Sediment Res.* **2018**, *33*, 157–170. [CrossRef]
26. Shafizadeh-Moghadam, H.; Valavi, R.; Shahabi, H.; Chapi, K.; Shirzadi, A. Novel forecasting approaches using combination of machine learning and statistical models for flood susceptibility mapping. *J. Environ. Manag.* **2018**, *217*, 1–11. [CrossRef]
27. Janizadeh, S.; Kim, D.; Jun, C.; Bateni, S.M.; Pandey, M.; Mishra, V.N. Impact of climate change on future flood susceptibility projections under shared socioeconomic pathway scenarios in South Asia using artificial intelligence algorithms. *J. Environ. Manag.* **2024**, *366*, 121764. [CrossRef]
28. Tăban, C.I.; Sandu, A.; Oancea, S.; Stoia, M. Gross Alpha/Beta Radioactivity of Drinking Water and Relationships with Quality Parameters of Water from Alba County, Romania. *Rom. J. Phys.* **2024**, *69*, 806.
29. Chirosca, G.; Mihailov, M.A.; Tomescu-Chivu, M.I.; Chirosca, A.V. Enhanced Machine Learning Model for Meteo-Oceanographic Time-Series Prediction. *Rom. J. Phys.* **2022**, *67*, 815.
30. Nichita, C.; Voinea, S. Removal of the pharmaceutical pollutants from water using natural filter materials-experimental lab. *Rom. Rep. Phys.* **2024**, *76*, 706. [CrossRef]
31. Costache, R.; Bărbulescu, A.; Pham, Q.B. Integrated Framework for Detecting the Areas Prone to Flooding Generated by Flash-Floods in Small River Catchments. *Water* **2021**, *13*, 758. [CrossRef]
32. Costache, R.; Țîncu, R.; Elkhrachy, I.; Pham, Q.B.; Popa, M.C.; Diaconu, D.C.; Avand, M.; Costache, I.; Arabameri, A.; Bui, D.T. New neural fuzzy-based machine learning ensemble for enhancing the prediction accuracy of flood susceptibility mapping. *Hydrol. Sci. J.* **2020**, *65*, 2816–2837. [CrossRef]
33. Costache, R.; Pham, Q.B.; Avand, M.; Linh, N.T.T.; Vojtek, M.; Vojteková, J.; Lee, S.; Khoi, D.N.; Nhi, P.T.T.; Dung, T.D. Novel hybrid models between bivariate statistics, artificial neural networks and boosting algorithms for flood susceptibility assessment. *J. Environ. Manag.* **2020**, *265*, 110485. [CrossRef] [PubMed]

34. Popescu, N.C.; Bărbulescu, A. On the flash flood susceptibility and accessibility in the Vărbilău catchment (Romania). *Rom. J. Phys.* **2022**, *67*, 811.
35. Popescu, C.; Bărbulescu, A. Flood Hazard Evaluation using a Flood Potential Index. *Water* **2023**, *15*, 3533. [CrossRef]
36. Stancu, M.V.; Chevereșan, M.I.; Sârbu, D.; Maizel, A.; Soare, R.; Bărbulescu, A.; Dumitriu, C.S. Influence of marine currents, waves and shipping traffic on Sulina channel fairway at the mouth of Black Sea. *Water* **2024**, *16*, 2779. [CrossRef]
37. Crăciun, A.; Costache, R.; Bărbulescu, A.; Chandra Pal, S.; Costache, I.; Dumitriu, C.S. Modern techniques for flood susceptibility estimation across the Deltaic Region (DD) from the Black Sea's Romanian Sector. *J. Mar. Sci. Eng.* **2022**, *10*, 1149. [CrossRef]
38. Carey, S.K.; Woo, M. Slope runoff processes and flow generation in a subarctic, subalpine catchment. *J. Hydrol.* **2001**, *253*, 110–129. [CrossRef]
39. Bakuła, K.; StĘpnik, M.; Kurczyński, Z. Influence of elevation data source on 2D hydraulic modelling. *Acta Geophys.* **2016**, *64*, 1176–1192. [CrossRef]
40. Allahbakhshian-Farsani, P.; Vafakhah, M.; Khosravi-Farsani, H.; Hertig, E. Regional flood frequency analysis through some machine learning models in semi-arid regions. *Water Resour. Manag.* **2020**, *34*, 2887–2909. [CrossRef]
41. Biswas, M.; Banerji, S.; Mitra, D. Land-use–land-cover change detection and application of Markov model: A case study of Eastern part of Kolkata. *Environ. Dev. Sustain.* **2020**, *22*, 4341–4360. [CrossRef]
42. Kononenko, I.; Kukar, M. *Machine Learning and Data Mining*; Woodhead Publishing: Swaston, UK, 2007; pp. 153–180.
43. Saaty, T.L. Decision making with the analytic hierarchy process. *Int. J. Serv. Sci.* **2008**, *1*, 83–98. [CrossRef]
44. Hasanuzzaman, M.; Adhikary, P.P.; Bera, B.; Shit, P.K. Flood vulnerability assessment using AHP and frequency ratio techniques. In *Spatial Modelling of Flood Risk and Flood Hazards: Societal Implications*; Pradhan, B., Shit, P.K., Bhunia, G.S., Adhikary, P.P., Pourghasemi, H.R., Eds.; Springer International Publishing: Cham, Switzerland, 2022; pp. 91–104.
45. Sejnowski, T.J. *The Deep Learning Revolution*; The MIT Press: Cambridge, MA, USA, 2018.
46. Chan, K.Y.; Abu-Salih, B.; Qaddoura, R.; Al-Zoubi, A.M.; Palade, V.; Pham, D.-S.; Del Ser, J.; Muhammad, K. Deep neural networks in the cloud: Review, applications, challenges and research directions. *Neurocomputing* **2023**, *545*, 126327. [CrossRef]
47. Smola, A.J.; Schölkopf, B. A tutorial on support vector regression. *Stat. Comput.* **2004**, *14*, 199–222. [CrossRef]
48. Park, Y.-S.; Lek, S. Chapter 7—Artificial neural networks: Multilayer Perceptron for Ecological Modeling. In *Developments in Environmental Modelling*; Jørgensen, S.E., Ed.; Elsevier: Amsterdam, The Netherlands, 2016; Volume 28, pp. 123–140.
49. Matsuki, Y.; Nakamura, K.; Watanabe, H.; Aoki, T.; Nakata, H.; Katsuragawa, S.; Doi, K. Usefulness of an artificial neural network for differentiating benign from malignant pulmonary nodules on high-resolution CT: Evaluation with receiver operating characteristic analysis. *Am. J. Roentgenol.* **2002**, *178*, 657–663. [CrossRef]
50. Ali, S.A.; Parvin, F.; Pham, Q.B.; Vojtek, M.; Vojteková, J.; Costache, R.; Linh, N.T.T.; Nguyen, H.Q.; Ahmad, A.; Ghorbani, M.A. GIS-based comparative assessment of flood susceptibility mapping using hybrid multi-criteria decision-making approach, naïve Bayes tree, bivariate statistics and logistic regression: A case of Topľa basin, Slovakia. *Ecol. Indic.* **2020**, *117*, 106620. [CrossRef]
51. Tehrany, M.S.; Pradhan, B.; Jebur, M.N. Flood susceptibility analysis and its verification using a novel ensemble support vector machine and frequency ratio method. *Stoch. Environ. Res. Risk Assess.* **2015**, *29*, 1149–1165. [CrossRef]